

Dirty bosons in a quasi-one-dimensional harmonic trap

Tama Khellil,^{1,*} Antun Balaž,^{2,†} and Axel Pelster^{3,‡}

¹*Institut für Theoretische Physik, Freie Universität Berlin, Arnimallee 14, 14195 Berlin, Germany*

²*Scientific Computing Laboratory, Institute of Physics Belgrade,
University of Belgrade, Pregrevica 118, 11080 Belgrade, Serbia*

³*Fachbereich Physik und Forschungszentrum OPTIMAS,
Technische Universität Kaiserslautern, 67663 Kaiserslautern, Germany*

The emergence of a Bose-glass phase in a quasi one-dimensional Bose-Einstein-condensed gas in a harmonic trapping potential with an additional delta-correlated disorder potential at zero temperature is studied using three approaches. At first, the corresponding time-independent Gross-Pitaevskii equation is numerically solved for the condensate wave function, and disorder ensemble averages are evaluated. In particular, we analyze quantitatively the emergence of mini-condensates in the local minima of the random potential, which occurs for weak disorder preferentially at the border of the condensate, while for intermediate disorder strength this happens in the trap center. Second, in view of a more detailed physical understanding of this phenomenon, we extend a quite recent non-perturbative approach towards the weakly interacting dirty boson problem, which relies on the Hartree-Fock theory and is worked out on the basis of the replica method, from the homogeneous case to a harmonic confinement. Finally, in the weak disorder regime we also apply the Thomas-Fermi approximation, while in the intermediate disorder regime we additionally use a variational ansatz in order to describe analytically the numerically observed redistribution of the fragmented mini-condensates with increasing disorder strength.

PACS numbers: 67.85.Hj, 05.40.-a, 03.75.Hh, 71.23.-k

I. INTRODUCTION

The dirty boson problem is defined as a system of interacting bosons in a random potential [1]. The combined effect of disorder and two-particle interaction represents one of the most challenging problems in condensed matter physics due to the intriguing interplay between localization and superfluidity. Cold atoms provide a controlled experimental setup in which that fundamental question of interacting bosons in a random environment can be addressed in both a quantitative and a tunable way.

The earliest relevant experiments, which were central for motivating the research of the dirty boson problem, dealt with superfluidity of thin films of ^4He adsorbed in porous Vycor glass in the low-density limit [2]. There it was proven that, despite the presence of disorder, superfluidity can still persist. For ultracold Bose gases disorder appears either naturally as, e.g., in magnetic wire traps [3–7], where imperfections of the wire itself can induce local disorder, or it may be created artificially and controllably as, e.g., by using laser speckle fields [8–12]. A set-up more in the spirit of condensed matter physics relies on a Bose gas with impurity atoms of another species trapped in a deep optical lattice, so the latter represent randomly distributed scatterers [13, 14]. Furthermore, an incommensurate optical lattice can provide a pseudo-random potential for an ultracold Bose gas [15–17].

Non-interacting particles in a random environment can be localized provided that the disorder is sufficiently strong. This phenomenon of Anderson localization occurs as the particles are repeatedly reflected back in the random potential, so interferences yield exponentially localized one-body wave functions [18]. In one dimension Anderson localization was experimentally found in an ultracold Bose gas in Refs. [12, 17]. Within a Bose-Einstein condensation (BEC), which is a many-particle interacting system, the presence of disorder causes the emergence of a new phase besides the superfluid phase (SF), which is called a Bose-glass phase due to the localization of bosons in the respective minima of the random potential landscape. This Bose-glass phase contains no superfluid fraction and is characterized by a finite compressibility, by the absence of a gap, and by an infinite superfluid susceptibility [1]. Indications for the existence of the Bose-glass phase were found, for instance, in the experiments of Refs. [7, 8]. There it was shown within the superfluid phase that an increasing disorder strength yields first a fragmentation of the condensate due to the formation of tiny BEC droplets in the minima of the random environment. For sufficiently strong disorder the condensate then turns out to be completely destroyed as all bosons are localized in the minima of the random potential, which represents the Bose-glass phase. But a more quantitative investigation of that elusive phase is still lacking both from an experimental and a theoretical point of view.

One of the first important theoretical results of the dirty boson problem was obtained by Huang and Meng in 1992 [19]. Within a Bogoliubov theory for a weakly interacting Bose-Einstein condensate it was found that

*Electronic address: khellil.lpth@gmail.com

†Electronic address: antun.balaz@ipb.ac.rs

‡Electronic address: axel.pelster@physik.uni-kl.de

a weak random disorder potential leads to a depletion of both the global condensate density and the superfluid density due to the localization of bosons in the respective minima of the random potential [19–28]. Beyond the weak disorder, a perturbative approach was worked out in Refs. [29, 30], where the impact of the external random potential upon the quantum fluctuations was studied in detail. In order to analyze the BEC in the strong disorder regime, there are, in principle, two complementary non-perturbative approaches. The first starts from the superfluid phase and ends up in the Bose-glass phase for increasing disorder strength. To this end Ref. [31] applies the random phase approximation and yields a self-consistent integral equation for the disorder-averaged particle density, whereas Refs. [32, 33] work out a stochastic self-consistent mean-field approach using two chemical potentials, one for the condensed and one for the excited particles. The second approach starts conversely from the Bose-glass phase and proceeds towards the superfluid phase for decreasing disorder strength. For instance, Refs. [34, 35] work this out on the basis of a careful energetic analysis, where the disorder turns out to strongly influence the size, shape, and structure of the mini-condensates in the minima of the random potential. Furthermore, an order parameter was introduced and applied in the context of a Hartree-Fock theory in Ref. [36] in order to describe the emergence of the Bose-glass phase. But still there is a lack of investigation concerning the emergence of the Bose-glass phase and its properties.

In the present paper we treat the problem of a quasi-one-dimensional trapped BEC in a disorder potential both analytically and numerically. We start first by describing the underlying BEC model and by developing a Hartree-Fock mean-field theory for the weak disorder regime in Section II. Concerning the numerical treatment in Section III, we solve the corresponding Gross-Pitaevskii (GP) equation of the BEC model and perform disorder-ensemble averages of the condensate wave function. Then we apply a variational ansatz for the intermediate disorder regime in Section IV. Those three different methods are then compared in Section V. In particular, we discuss the respective results for the particle density, which turns out to be decomposed into the condensate density and the density of fragmented local Bose-Einstein condensates within the respective minima of the random potential landscape.

II. HARTREE-FOCK MEAN-FIELD THEORY IN 1D

The model of a three-dimensional weakly interacting homogeneous Bose gas in a δ -correlated disorder potential was studied within the Hartree-Fock mean-field theory in Ref. [36] by applying the Parisi replica method [37–39]. As a result, the corresponding phase diagram for the occurrence of the superfluid, the Bose-glass, and the

normal phase was determined in the control parameter plane spanned by disorder strength and temperature. By applying the Thomas-Fermi approximation, this Hartree-Fock theory is extended in Ref. [40] to a harmonic confinement, and is applied here to one-dimensional systems.

Let us briefly summarize the main result of Ref. [40], which relies on deriving an approximation for the underlying free energy.

A. Free Energy

The starting point is the functional integral for the grand-canonical partition function

$$\mathcal{Z} = \oint \mathcal{D}\psi^* \oint \mathcal{D}\psi e^{-\mathcal{A}[\psi^*, \psi]/\hbar}, \quad (1)$$

where the integration is performed over all Bose fields $\psi^*(x, \tau), \psi(x, \tau)$, which are periodic in imaginary time τ , i.e., $\psi(x, \tau) = \psi(x, \tau + \hbar\beta)$. The Euclidean action is given in standard notation by

$$\begin{aligned} \mathcal{A}[\psi^*, \psi] = & \int_0^{\hbar\beta} d\tau \int dx \{ \psi^*(x, \tau) \left[\hbar \frac{\partial}{\partial \tau} - \frac{\hbar^2}{2M} \Delta \right. \right. \\ & \left. \left. + V(x) + U(x) - \mu \right] \psi(x, \tau) + \frac{1}{2} \int dx' \psi^*(x, \tau) \psi(x, \tau) \right. \\ & \left. \times V^{(\text{int})}(x - x') \psi^*(x', \tau) \psi(x', \tau) \right\}, \end{aligned} \quad (2)$$

where $V(x) = M\Omega^2 x^2/2$ denotes the harmonic trap with the trap frequency Ω , M the particle mass, μ the chemical potential, and $V^{(\text{int})}(x - x') = g\delta(x - x')$ the contact interaction potential. The interaction coupling strength $g = 2a\hbar\omega_r$ depends on the s-wave scattering length a , which has to be positive in order to obtain a stable BEC, and the transversal trap frequency ω_r . Note that the latter has to be large enough, i.e., $\omega_r \gg \Omega$, in order to ensure a quasi-one-dimensional setup [41, 42].

We assume for the disorder potential $U(x)$ that it is homogeneous after performing the disorder ensemble average (denoted by $\overline{\cdot}$) over all possible realizations. Thus, the expectation value of the disorder potential can be set to vanish without loss of generality

$$\overline{U(x)} = 0, \quad (3)$$

and its correlation function reads

$$\overline{U(x_1)U(x_2)} = D \delta(x_1 - x_2), \quad (4)$$

where D denotes the disorder strength.

Within the Hartree-Fock mean-field approximation with the replica method, Ref. [40] obtains self-consistency equations, which determine the particle density $n(x)$ as well as the order parameter of the superfluid $n_0(x)$, which represents the condensate density, and the order parameter of the Bose-glass phase $q(x)$, which stands for the density of the particles being condensed in the respective minima of the disorder potential.

More precisely, the two order parameters $n_0(x)$ and $q(x)$ of our mean-field theory at $T = 0$ are defined by following the notion of spin-glass theory [43, 45, 46]. The

off-diagonal long-range limit defines the condensate density [44]

$$\lim_{|x-x'|\rightarrow\infty} \overline{\langle\psi(x,\tau)\psi^*(x',\tau)\rangle} = n_0(x). \quad (5)$$

However, the Bose-glass order parameter $q(x)$ was introduced in Ref. [36] in close analogy to the Edward-Anderson order parameter of spin-glasses [47] according to

$$\lim_{|x-x'|\rightarrow\infty} \overline{|\langle\psi(x,\tau)\psi^*(x',\tau)\rangle|^2} = [n_0(x) + q(x)]^2. \quad (6)$$

In the one-dimensional case and at $T = 0$, the mean-field Hartree-Fock theory with the help of the replica method leads to the free energy [40]:

$$\begin{aligned} \mathcal{F} = & \int dx \left\{ -g[q(x) + n_0(x)]^2 - \frac{g}{2}n_0^2(x) - \sqrt{n_0(x)} \right. \\ & \left\{ \mu + \frac{\hbar^2}{2M} \frac{\partial^2}{\partial x^2} - 2g[q(x) + n_0(x)] - \frac{1}{2}M\Omega^2x^2 \right. \\ & \left. + \frac{D}{\hbar}Q_0(x) \right\} \sqrt{n_0(x)} + \frac{D}{\hbar}Q_0(x)[q(x) + n_0(x)] - \frac{D}{\hbar}\sqrt{\frac{M}{2}} \right. \\ & \left. \frac{[q(x) + n_0(x)]}{\sqrt{-\mu + 2g[q(x) + n_0(x)] + \frac{1}{2}M\Omega^2x^2 - \frac{D}{\hbar}Q_0(x)}} \right\}. \quad (7) \end{aligned}$$

Here $Q_0(x)$ represents an auxiliary function within the Hartree-Fock theory. From the thermodynamic relation $-\frac{\partial\mathcal{F}}{\partial\mu} = N$ we obtain

$$\int_{-\infty}^{\infty} n(x)dx = N, \quad (8)$$

which defines the particle density $n(x)$.

Extremising the free energy (7) with respect to the functions $q(x)$, $n_0(x)$, and $Q_0(x)$, i.e., $\frac{\delta\mathcal{F}}{\delta n_0(x')} = 0$, $\frac{\delta\mathcal{F}}{\delta Q_0(x')} = 0$, and $\frac{\delta\mathcal{F}}{\delta q(x')} = 0$, respectively, yields together with Eq. (8) four coupled self-consistency equations: an algebraic equation for the Bose-glass order parameter $q(x)$,

$$q(x) = \frac{D}{\hbar M}Q_0^3(x) \frac{n_0(x)}{1 - \frac{D}{\hbar M}Q_0^3(x)}, \quad (9)$$

a nonlinear differential equation for the condensate density $n_0(x)$,

$$\begin{aligned} & \left[-\mu + 2gn(x) + V(x) - gn_0(x) - \frac{D}{\hbar}Q_0(x) \right. \\ & \left. - \frac{\hbar^2}{2M} \frac{\partial^2}{\partial x^2} \right] \sqrt{n_0(x)} = 0, \quad (10) \end{aligned}$$

and the sum of them which is the total density $n(x)$,

$$n(x) = q(x) + n_0(x), \quad (11)$$

while the auxiliary function $Q_0(x)$ turns out to be the solution of the cubic equation

$$-\frac{D}{\hbar}Q_0^3(x) + [-\mu + 2gn(x) + V(x)]Q_0^2(x) - \frac{M}{2} = 0. \quad (12)$$

We deal now first with the homogeneous Bose gas and treat later on the harmonic confinement via the Thomas-Fermi approximation.

B. Homogeneous Case

The simplest case to discuss is the homogeneous one, where $V(x) = 0$. Since all densities are spatially constant in the homogeneous case, we drop in this section the x dependency of all densities. With this, Eqs. (9)–(11) reduce, after eliminating Q_0 , to:

$$q = \frac{D}{\hbar M} \frac{n_0}{\left(\frac{2gn_0}{M}\right)^{\frac{3}{2}} - \frac{D}{\hbar M}}, \quad (13)$$

$$gn_0 = -\mu + 2gn - \frac{D}{\hbar} \sqrt{\frac{M}{2gn_0}}, \quad (14)$$

$$n = q + n_0. \quad (15)$$

From Eqs. (15) and (13) we get an algebraic fifth-order equation for the condensate fraction n_0/n :

$$\left(\frac{n_0}{n}\right)^{5/2} - \left(\frac{n_0}{n}\right)^{3/2} + \overline{D} = 0, \quad (16)$$

where $\overline{D} = \frac{\xi^3}{\mathcal{L}^3}$ denotes the dimensionless disorder strength, $\xi = \frac{\hbar}{\sqrt{2Mgn}}$ the coherence length, and $\mathcal{L} = \left(\frac{\hbar^4}{M^2D}\right)^{1/3}$ the Larkin length [34, 48]. Figure 1 shows how the condensate fraction n_0/n decreases with increasing the dimensionless disorder strength \overline{D} according to Eq. (16). Thus, the mean-field theory predicts a first-order quantum phase transition from the superfluid phase to the Bose-glass phase at the critical value $\overline{D}_c = \frac{6}{25}\sqrt{\frac{3}{5}} \simeq 0.185$. This corresponds to the value $\overline{D}_c = 1$, that was found in the non-perturbative approach of Refs. [34, 35], which investigate at which disorder strength the Bose-glass phase becomes energetically unstable and goes over into the superfluid phase. Therefore, we expect that a quantum phase transition will also appear in the trapped case within the Thomas-Fermi approximation.

Now we check whether our results are compatible with the Huang-Meng theory [19–28], where the Bose-glass order parameter of a homogeneous dilute Bose gas at zero temperature in case of weak disorder regime is deduced within the seminal Bogoliubov theory. The Bose-glass order parameter in one dimension is according to

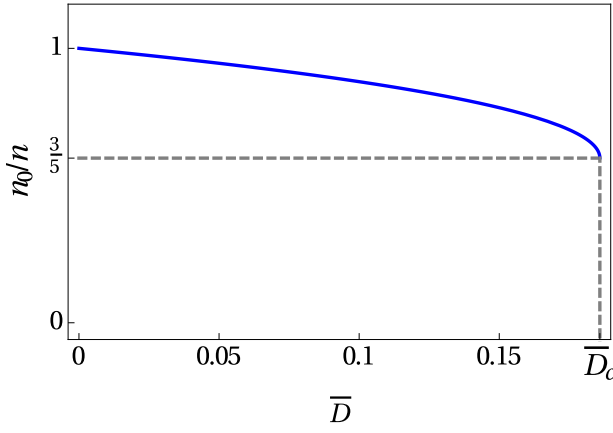


Figure 1: (Color online) Condensate fraction n_0/n as function of dimensionless disorder strength \bar{D} , as a solution of Eq.(16).

the Huang-Meng theory proportional to the disorder strength, which yields in dimensionless form

$$\frac{q_{\text{HM}}}{n} = \frac{\bar{D}}{2^{3/2}}. \quad (17)$$

In our Hartree-Fock mean-field theory the Bose-glass order parameter in case of weak disorder strength turns out to be

$$\frac{q_w}{n} = \bar{D}. \quad (18)$$

Thus, from Eq. (18) we conclude that the Huang-Meng theory is qualitatively valid. But quantitatively the comparison of Eqs. (17) and (18) reveals that a factor of $2^{3/2}$ is missing in our result (18). This is due to the fact that the Hartree-Fock theory does not contain the Bogoliubov channel, which is included in the Huang-Meng theory.

C. Thomas-Fermi Approximation

We deal now with the trapped case. The exact analytical solution of the differential equation (10) is impossible to obtain even in the absence of disorder. Therefore, we approximate its solution via the Thomas-Fermi (TF) approximation method, which is based on neglecting the kinetic energy.

It turns out that we have to distinguish between two different spatial regions: the superfluid region, where the bosons are distributed in the condensate as well as in the minima of the disorder potential, and the Bose-glass region, where there are no bosons in the global condensate so that all bosons contribute only to the local Bose-Einstein condensates. In the following the radius of the superfluid region, i.e., the condensate radius, is denoted by $R_{\text{TF}1}$, while the radius of the whole bosonic cloud $R_{\text{TF}2}$ is called the cloud radius.

Within the TF approximation the algebraic equations (9), (11), and (12) remain the same, but the differential equation (10) reduces to an algebraic relation in the superfluid region:

$$-\mu + 2gn(x) + V(x) - gn_0(x) - \frac{D}{\hbar}Q_0(x) = 0. \quad (19)$$

Outside the superfluid region, i.e., in the Bose-glass region, Eq. (10) reduces simply to $n_0(x) = 0$. The advantage of the TF approximation is that now we have only four coupled algebraic equations.

At first we consider the superfluid region. In the TF approximation the dependency on the auxiliary function $Q_0(x)$ in Eq. (12) can be eliminated and Eqs. (9), (11), and (19) reduce in the superfluid region to:

$$-\tilde{\mu} + 2\tilde{n}(\tilde{x}) + \tilde{x}^2 - \tilde{n}_0(\tilde{x}) - 2\frac{\tilde{D}}{\sqrt{\tilde{n}_0(\tilde{x})}} = 0, \quad (20)$$

$$\tilde{q}(\tilde{x}) = \tilde{D} \frac{\tilde{n}_0(\tilde{x})}{\tilde{n}_0^{3/2}(\tilde{x}) - \tilde{D}}, \quad (21)$$

$$\tilde{n}(\tilde{x}) = \tilde{q}(\tilde{x}) + \tilde{n}_0(\tilde{x}), \quad (22)$$

where $\tilde{n}(\tilde{x}) = n(x)/\bar{n}$ denotes the dimensionless total density, $\tilde{n}_0(\tilde{x}) = n_0(x)/\bar{n}$ the dimensionless condensate density, $\tilde{q}(\tilde{x}) = q(x)/\bar{n}$ the dimensionless Bose-glass order parameter, $\tilde{x} = x/R_{\text{TF}}$ the dimensionless coordinate, $\bar{n} = \bar{\mu}/g$ the maximal total density in the clean case, $\tilde{\mu} = \mu/\bar{\mu}$ the dimensionless chemical potential, $\tilde{D} = \frac{\xi^3}{\mathcal{L}^3}$ the dimensionless disorder strength, $\xi = \frac{l^2}{R_{\text{TF}}}$ the coherence length in the center of the trap, $l = \sqrt{\frac{\hbar}{M\Omega}}$ the oscillator length, and $R_{\text{TF}} = l\sqrt{\frac{2\bar{\mu}}{\hbar\Omega}}$ the TF cloud radius. The chemical potential in the absence of the disorder $\bar{\mu} = \hbar\omega_r \left(\frac{3}{2\sqrt{2}} N \frac{a}{l} \sqrt{\frac{\Omega}{\omega_r}} \right)^{2/3}$, which provides the energy scale, is deduced from the normalization condition (8) in the clean case, i.e., when $D = 0$.

Inserting Eqs. (21) and (22) into Eq. (20) gives us one self-consistency equation for the condensate density in the superfluid region:

$$\begin{aligned} \tilde{n}_0^3(\tilde{x}) + (-\tilde{\mu} + \tilde{x}^2) \tilde{n}_0^2(\tilde{x}) - \tilde{D} \tilde{n}_0^{3/2}(\tilde{x}) \\ - \tilde{D} (-\tilde{\mu} + \tilde{x}^2) \sqrt{\tilde{n}_0(\tilde{x})} + 2\tilde{D}^2 = 0. \end{aligned} \quad (23)$$

This equation is of sixth order with respect to $\sqrt{\tilde{n}_0(\tilde{x})}$, which makes it impossible to solve analytically. Therefore, we solve it numerically and insert the result into Eqs. (21) and (22) in order to determine the Bose-glass order parameter $\tilde{q}(\tilde{x})$ and the total density $\tilde{n}(\tilde{x})$, respectively.

Now we come to the Bose-glass region, where we have from Eq. (10) in TF approximation $\tilde{n}_0(\tilde{x}) = 0$, and Eq.

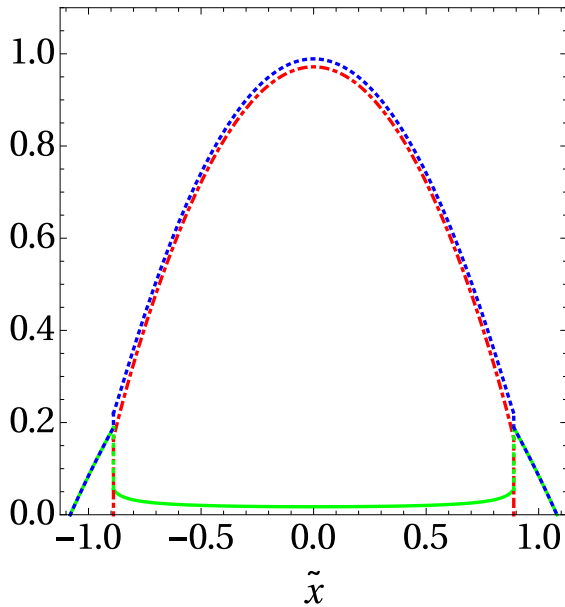


Figure 2: (Color online) Spatial distribution of the total particle density $\tilde{n}(\tilde{x})$ (dotted, blue), condensate density $\tilde{n}_0(\tilde{x})$ (dotted-dashed, red), and Bose-glass order parameter $\tilde{q}(\tilde{x})$ (solid green) for the dimensionless disorder strength $\tilde{D} = 0.016$.

(11) reduces to $\tilde{n}(\tilde{x}) = \tilde{q}(\tilde{x})$. Inserting this into Eq. (9), we get $Q_0(x) = \left(\frac{\hbar M}{D}\right)^{1/3}$, which reduces Eq. (12) to:

$$\tilde{q}(\tilde{x}) = \frac{1}{2} \left(3\tilde{D}^{2/3} + \tilde{\mu} - \tilde{x}^2 \right). \quad (24)$$

We also need to write down the dimensionless equivalent of the normalization condition (8), which reads:

$$\int_{-\tilde{R}_{\text{TF}2}}^{\tilde{R}_{\text{TF}2}} \tilde{n}(\tilde{x}) d\tilde{x} = \frac{4}{3}, \quad (25)$$

where $\tilde{R}_{\text{TF}2} = R_{\text{TF}2}/R_{\text{TF}}$ denotes the dimensionless cloud radius, and the total density $\tilde{n}(\tilde{x})$ in Eq. (25) is the combination of the total densities from both the superfluid region and the Bose-glass region.

D. Thomas-Fermi Results

Before considering any particular parameter value for our BEC system, we have first to justify using the TF approximation and determine its range of validity. To this end we rewrite Eq. (10) in the clean case, i.e., for $D = 0$, and divide it with $\tilde{\mu}$. This yields:

$$\left[-1 + \tilde{n}(\tilde{x}) + \tilde{x}^2 - \left(\frac{\xi}{R_{\text{TF}}} \right)^2 \frac{\partial^2}{\partial \tilde{x}^2} \right] \sqrt{\tilde{n}(\tilde{x})} = 0. \quad (26)$$

Note that in the clean case the total density coincides with the condensate one. The TF approximation is only

justified when the prefactor of the kinetic term $\left(\frac{\xi}{R_{\text{TF}}}\right)^2$ is small enough, so the kinetic term can be neglected, which yields

$$\xi \ll R_{\text{TF}}. \quad (27)$$

In this paper we perform our study for ^{87}Rb atoms and for the following experimentally realistic parameters: $N = 10^6$, $\Omega = 2\pi \times 50 \text{ Hz}$, $\omega_r = 2\pi \times 179 \text{ Hz}$, and $a = 100 a_0$, where a_0 is the Bohr radius. For those parameters the oscillator length reads $l = 1.5250.9 \mu\text{m}$, the coherence length in the trap center turns out to be $\xi = 45.6 \text{ nm}$, and the Thomas-Fermi radius reads $R_{\text{TF}} = 50.9 \mu\text{m}$, so the assumption (27) for the TF approximation is, indeed, fulfilled. Furthermore, the transverse oscillator length $l_r = \sqrt{\frac{\hbar}{M\omega_r}} = 806.04 \text{ nm}$ is much larger than the scattering length, i.e., $a \ll l_r$, but still smaller than the longitudinal oscillator length $l = 1.52 \mu\text{m}$, so we are in the quasi one-dimensional regime [41, 42].

Using those parameter values we solve equation Eq. (23) numerically. To this end we select from all real solutions the physical one, i.e., the one with the smallest energy. Then we combine the superfluid region solution with Eq. (24) describing the Bose-glass region. After that we fix the chemical potential $\tilde{\mu}$ using the normalization condition (25). The resulting densities are combined and plotted in Fig. 2.

We read off from Fig. 2 that the total density $\tilde{n}(\tilde{x})$ vanishes at the cloud radius, and reveals a tiny jump at the condensate radius. The condensate density $\tilde{n}_0(\tilde{x})$ jumps to zero at the condensate radius, which separates the superfluid region from the Bose-glass one. The Bose-glass order parameter $\tilde{q}(\tilde{x})$ has a double-bump structure and vanishes at the cloud radius. In the Bose-glass region, the Bose-glass order parameter and the total density are on top of each other. Thus, the three densities turn out not to be continuous at the condensate radius, which is an artifact of the applied TF approximation. To study the influence of the disorder on the BEC, we plot the resulting TF radii in Fig. 3(a) as a function of the disorder strength \tilde{D} . The dimensionless condensate radius $\tilde{R}_{\text{TF}1} = R_{\text{TF}1}/R_{\text{TF}}$ is defined as the radius at which the condensate density determined from (23) so that, equation $\frac{\partial \tilde{x}}{\partial \tilde{n}_0(\tilde{x})}|_{\tilde{x}=\tilde{R}_{\text{TF}1}} = 0$ has to be solved. Correspondingly, the dimensionless cloud radius $\tilde{R}_{\text{TF}2}$ is defined by the condition that the solution of Eq. (24) vanishes, i.e., $3\tilde{D}^{2/3} + \tilde{\mu} - \tilde{R}_{\text{TF}2}^2 = 0$. We distinguish two different phases, the superfluid one and the Bose-glass one. We see that both cloud and condensate radius coincide in the clean case. The condensate radius decreases with increasing the disorder strength and vanishes at the critical value $D_c = 0.143$, which marks a quantum phase transition from the superfluid to the Bose-glass phase. This corresponds to the value $\tilde{D}_c = 0.333$, which was found in the non-perturbative approach of Refs. [34, 35] to be the critical disorder strength, where the Bose-glass phase becomes energetically unstable and goes over into the superfluid phase. On the other side the cloud radius $\tilde{R}_{\text{TF}2}$

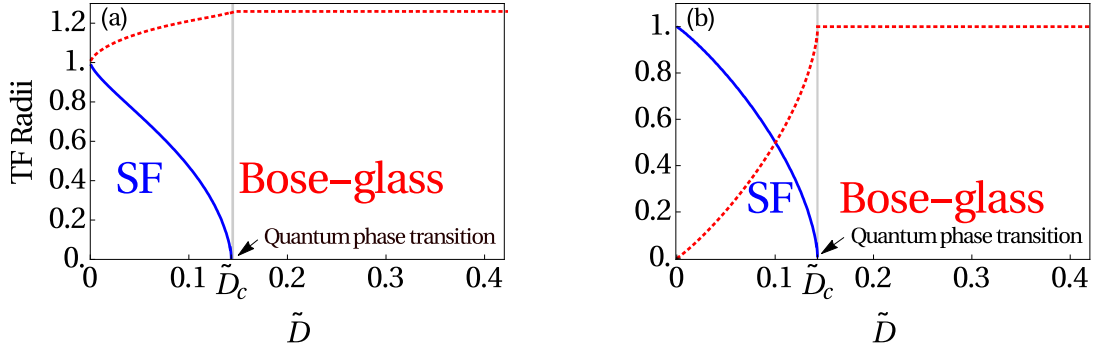


Figure 3: (Color online) (a) Cloud radius \tilde{R}_{TF2} (dotted, red) and condensate radius \tilde{R}_{TF1} (solid, blue), (b) Fractional number of condensed particles N_0/N (solid, blue) and disconnected local minicondensates Q/N (dotted, red) as functions of the dimensionless disorder strength \tilde{D} reveal a quantum phase transition from a superfluid (SF) to the Bose-glass phase.

increases with the disorder in the superfluid phase, but remains constant in the Bose-glass phase at the value $\tilde{R}_{\text{TF2}} = 1.256$. This means that beyond the critical disorder strength \tilde{D}_c the bosonic cloud is not extending anymore and has a maximal size. The same conclusion can be deduced from Fig. 3(b), where we depict the fractional number of the condensate $N_0/N = \frac{3}{4} \int_{-\tilde{R}_{\text{TF1}}}^{\tilde{R}_{\text{TF1}}} \tilde{n}_0(\tilde{x}) d\tilde{x}$. Here N_0/N equals to one in the clean case, i.e., all particles are in the condensate. Afterwards it decreases as the disorder strength \tilde{D} is increased, until it vanishes at \tilde{D}_c , marking the end of the superfluid phase and the beginning of the Bose-glass phase. Conversely behaves the fraction in the disconnected mini-condensates $Q/N = \frac{3}{4} \int_{-\tilde{R}_{\text{TF2}}}^{\tilde{R}_{\text{TF2}}} \tilde{q}(\tilde{x}) d\tilde{x}$, where Q stands for the number of particles in the disconnected mini-condensates. It increases with the increasing disorder until reaching the maximal value unity at \tilde{D}_c , then it remains to be one in the Bose-glass phase since all particles are stuck in the minima of the disorder potential.

III. NUMERICAL TREATMENT

Now we perform a numerical study for the Bose-condensed gas in one dimension at zero temperature in a harmonic trapping potential $V(x) = \frac{1}{2}M\Omega^2x^2$. Furthermore, we assume a Gaussian-distributed disorder potential $U(x)$, which satisfies the conditions

$$\overline{U(x)} = 0, \quad (28)$$

and

$$\overline{U(x)U(x')} = D(x - x') = \frac{D}{\sqrt{2\pi\lambda}} e^{-\frac{(x-x')^2}{2\lambda^2}}, \quad (29)$$

where $D(x - x')$ denotes the correlation function, λ the correlation length, and D the disorder strength. Note that the analytical study in Section II is done for δ -correlated disorder, but since it is impossible to treat the δ -correlated disorder numerically, we use the

Gaussian-distributed disorder (29), which specializes to a δ -distributed one in the limit $\lambda \rightarrow 0$, i.e., $\lim_{\lambda \rightarrow 0} D(x) = D\delta(x)$.

A one-dimensional BEC in the mean-field Hartree approximation is given by a generalized time-independent Gross-Pitaevskii equation for the ground-state wave function $\psi(x)$:

$$\left[-\frac{\hbar^2}{2M} \frac{\partial^2}{\partial x^2} - \mu + U(x) + V(x) + g\psi^*(x)\psi(x) \right] \psi(x) = 0. \quad (30)$$

Equation (30) represents a stochastic nonlinear differential equation which can not be solved exactly, and, therefore, we apply a numerical approach. To this end we have first to generate the random potential $U(x)$ before inserting it into Eq. (30), and then calculate the disorder average over many realizations of $U(x)$.

A. Generating Random Potential

Motivated by Fourier series, a simple ansatz for generating a random function $U(x)$ is performed as follows. The potential is written as a finite superposition of $\sin kx$ and $\cos kx$ terms with properly selected amplitudes A_n , B_n , and wave numbers k_n [49, 50]:

$$U(x) = \frac{1}{\sqrt{N}} \sum_{n=0}^{N-1} (A_n \cos k_n x + B_n \sin k_n x), \quad (31)$$

where N denotes the number of terms, which should be large enough in order to obtain a good approximation for the random potential. Furthermore, we assume A_n and B_n to be mutually independent Gaussian-correlated random variables with zero mean, and variance equal to $D(0)$:

$$\overline{A_n B_n} = 0, \quad \overline{A_n A_m} = \overline{B_n B_m} = D(0)\delta_{nm}. \quad (32)$$

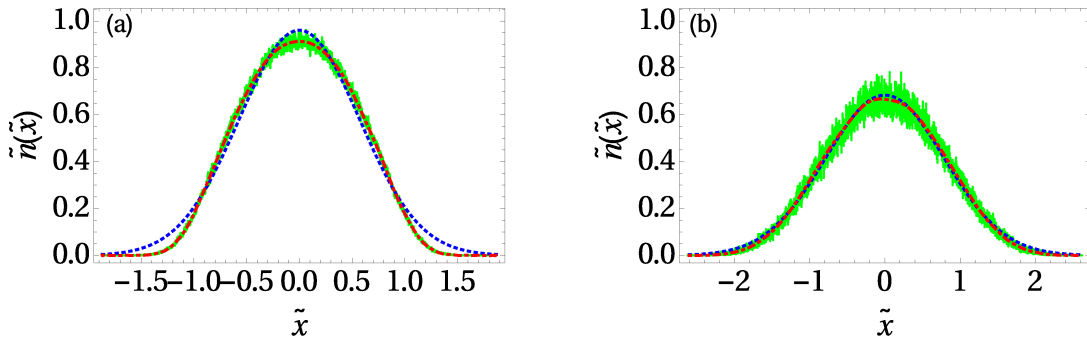


Figure 4: (Color online) Spacial distribution of the particle density $\tilde{n}(\tilde{x})$: numerical data (solid, green), fitted curve (dotted-dashed, red), and fitted Gaussian (dotted, blue) for (a) $\tilde{D} = 0.067$ and (b) $\tilde{D} = 0.603$.

The wave numbers k_n are independent random variables, as well, selected from the probability distribution:

$$p(k_n) = \frac{S(k_n)}{\int_{-\infty}^{\infty} S(k') dk'}, \quad (33)$$

where $S(k)$ defines the spectral density as the Fourier transform of the correlation function:

$$S(k) = \int_{-\infty}^{\infty} dx e^{-ikx} D(x). \quad (34)$$

In the special case of the Gaussian correlated disorder (29), the probability distribution (33) reads:

$$p(k_n) = \frac{\lambda}{\sqrt{2\pi}} e^{-\frac{\lambda^2 k_n^2}{2}}, \quad (35)$$

In order to numerically generate the correlation function (29) with sufficient accuracy, two numbers have to be appropriately large enough. The first one is the number N of terms in Eq. (31), the second one is the number M of realizations of the disorder potential, which are used to evaluate the disorder ensemble average (29). It can be shown analytically that the error in reproducing the correlation function (29) in the case $M \rightarrow \infty$ is of the order of $1/N$ [50]. All Gaussian-correlated quantities are generated using the Box-Müller algorithm [51].

B. Numerical Results

We insert the generated disorder potential (31) into the Gross-Pitaevskii Eq. (30), and then use a C computer program that solves the time-independent Gross-Pitaevskii equation in one space dimension in a harmonic trap using the imaginary-time propagation [52–54]. In this way we obtain the numerical solution of the ground-state wave function $\psi(x)$ of Eq. (30) for $M = 1000$ realizations of the disorder potential and $N = 10000$ terms in Eq. (31). To this end we use different values of the disorder strength D in order to cover the range from the weak

to the intermediate disorder regime. We have chosen the disorder correlation length to be $\lambda = 0.01 l$, which is small enough in order to approach the case of δ -correlated disorder.

Performing disorder ensemble averages, we have access to the particle density $n(x) = \psi(x)^2$, to the condensate density $n_0(x) = \overline{\psi(x)^2}$, and to the Bose-glass order parameter $q(x) = n(x) - n_0(x)$. In order to be able to compare the numerical results with the analytical ones obtained in Section II, we use the same rescaling parameters for all densities, coordinates, chemical potential, and disorder strength, which were already explained below Eq. (22).

Before discussing the numerical results in detail, we show first one typical example in Figs. 4, where the total density $\tilde{n}(\tilde{x})$ is plotted for two different values of the disorder strength (solid, green line), showing the original data for $M = 1000$ and $N = 10000$ terms in Eq. (31). We remark that the resulting density is fluctuating around a Gaussian-like curve. Comparing Fig. 4(a) with Fig. 4(b) we conclude that the fluctuations are increasing with the disorder strength. The origin of those fluctuations is that the $M = 1000$ realizations of the disorder potential for performing the disorder ensemble average are not sufficient to produce a smooth curve. One solution of this problem would be to increase the number M of the realizations of the disorder potential, which would need longer execution time, especially for the intermediate disorder regime, where the numerics has to be run for a larger spatial range. Another solution is to extract a continuous smooth curve that fits best to our data, as it is done in Fig. 4 (dotted-dashed, red line). This method is applied to all numerical densities in this paper. Furthermore, from the Gaussian fit in Fig. 4 (dotted, blue line), we remark that the original data of the total density approach a Gaussian form in the intermediate disorder regime much better than in the weak disorder regime. This can be explained with the argument that increasing the disorder reduces effectively the repulsive interaction between the particles and, thus, approaches the case of non-interacting bosons, where the total density is given

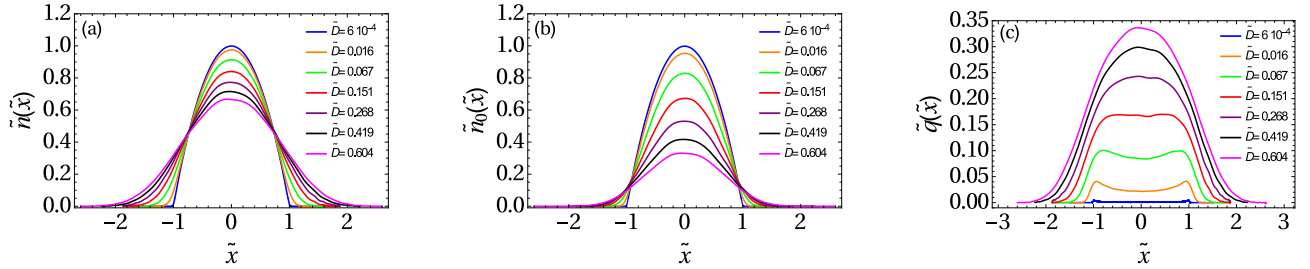


Figure 5: (Color online) Spatial distribution of: (a) particle density $\tilde{n}(\tilde{x})$, (b) condensate density $\tilde{n}_0(\tilde{x})$, and (c) Bose-glass order parameter $\tilde{q}(\tilde{x})$ for increasing disorder strengths \tilde{D} , from the top to the bottom in the center in (a) and (b), and from the bottom to the top in (c).

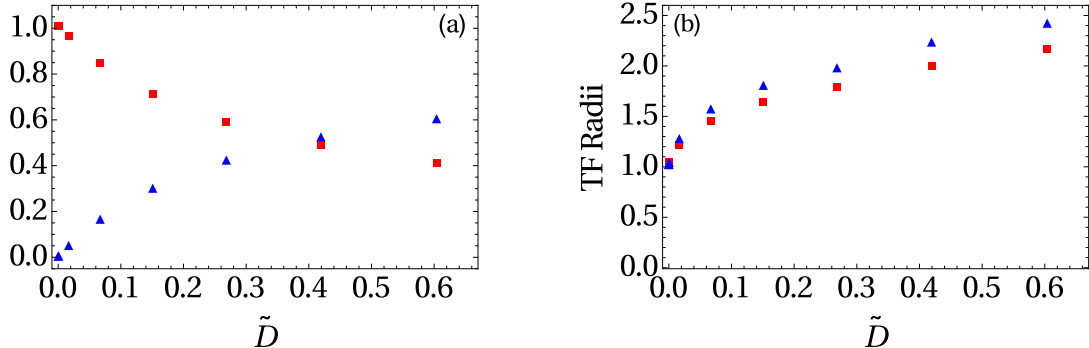


Figure 6: (Color online) (a) Fractional number of condensed particles N_0/N (square, red) and fractional number of particles Q/N in the disconnected local mini-condensates (triangle, blue), and (b) condensate radius $\tilde{R}_{\text{TF}1}$ (square, red) and cloud radius $\tilde{R}_{\text{TF}2}$ (triangle, blue) as function of disorder strength \tilde{D} .

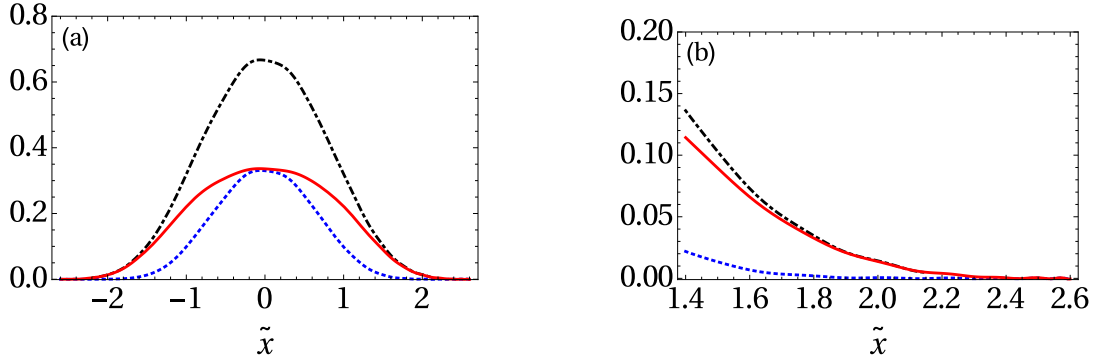


Figure 7: (Color online) Spatial distribution of: (a) particle density $\tilde{n}(\tilde{x})$ (dotted-dashed, black), condensate density $\tilde{n}_0(\tilde{x})$ (dotted, blue), Bose-glass order parameter $\tilde{q}(\tilde{x})$ (solid, red) and (b) blow-up of the border region for $\tilde{D} = 0.604$.

by a Gaussian.

In Fig. 5(a) the total density has a Gaussian-like form. The width of the total density, which is the spatial range where the total density is not vanishing, is increasing with the disorder strength and the bosonic cloud is becoming larger, while the maximal total density is decreasing with the disorder strength. Figure. 5(b) shows that the condensate density $\tilde{n}_0(\tilde{x})$ has qualitatively the same behavior as the total density $\tilde{n}(\tilde{x})$. In order to obtain a clearer picture, we plot in Fig. 6(a) the fractional number of the condensate $N_0/N = \frac{3}{4} \int \tilde{n}_0(\tilde{x}) d\tilde{x}$ as a function of the dis-

order strength. This fraction decreases with the disorder strength, which means that more and more particles are leaving the condensate with increasing \tilde{D} . Unfortunately, the employed numerical algorithm breaks down for larger values of the disorder strength, and one would have to use other approaches in this case. Therefore we focus on the regimes of weak to moderate disorder.

The Bose-glass order parameter is also plotted for different values of \tilde{D} in Fig. 5(c) but it has a complete different behavior than the two previous densities $\tilde{n}(\tilde{x})$ and $\tilde{n}_0(\tilde{x})$. In the weak disorder regime, $\tilde{q}(\tilde{x})$ reveals a dou-

ble bump structure and is maximal at the border of the condensate, while in the intermediate disorder regime it has a Gaussian-like form. This redistribution takes place, according to Fig. 5(c), at a disorder strength value between $\tilde{D} = 0.151$ and $\tilde{D} = 0.268$. Thus, the main difference between the weak and the intermediate disorder regime is that the local condensates concentrate at the border of the condensate in the former case, but sit in the center in the latter case. However, both in the weak and the intermediate disorder regime the width as well as the maximum of the Bose-glass order parameter increase with the disorder. Also the fraction in the disconnected mini-condensates $Q/N = \frac{3}{4} \int \tilde{q}(\tilde{x}) d\tilde{x}$, plotted in Fig. 6(a), increases with the disorder strength, as more and more bosons are captured in the mini-condensates of the disorder potential.

In order to know if, due to the disorder, the Bose-glass region exists or not, we plot the three densities $n(x)$, $n_0(x)$, and $q(x)$ together in Fig. 7(a) for the relatively intermediate disorder value $\tilde{D} = 0.604$. Indeed the blow-up of the intermediate region in Fig. 7(b) reveals clearly that the condensate vanishes at the border of the bosonic cloud, while the Bose-glass order parameter still persists, so the superfluid and the Bose-glass region coexist in the trap.

Fig. 6(b) shows both the condensate radius and the cloud radius, which we define by the length where the condensate density and the total density are equal or smaller than 10^{-4} , respectively. Both are almost identical in the weak disorder regime, then they both increase linearly with the disorder strength. As the difference between cloud and condensate radius increases with \tilde{D} , the Bose-glass region, as shown in Fig. 7(b), becomes larger at intermediate disorder strength.

Comparing the analytical results of Section II with the numerical ones of this section yields that the TF approximation is valid only in the weak disorder regime especially in the center of the trap, where the kinetic energy can be neglected, but it does not represent a good approximation for intermediate disorder strengths. The origin of this invalidity is the fact that the condition (27) is not fulfilled in the intermediate disorder regime. The coherence length becomes significantly larger as we increase the disorder strength, especially at the border of the bosonic cloud, so when it becomes of the order of the Thomas-Fermi radius, the TF approximation breaks down. Furthermore, quantum fluctuations are more dominating in lower dimensions, which also restricts the validity range of the TF approximation. In order to have a global picture of the behavior of the dirty BEC, not only in the presence of weak disorder but also in the presence of stronger one, we use in the following section another approximation method to treat the dirty boson problem, which relies on a variational method.

IV. VARIATIONAL METHOD

Since the four self-consistency Eqs. (9)–(12) are obtained by extremising the free energy (7), we can apply

the variational method in the spirit of Refs. [55–58] to obtain approximate results. In order to be able to compare the variational results with the analytical and the numerical ones obtained in Sections II and III, respectively, we use the same rescaling parameters already introduced below Eq. (22) for all functions and parameters. To this end, we have to multiply (7) with the factor $1/(\bar{\mu}nR_{\text{TF}})$ to obtain:

$$\tilde{\mathcal{F}} = \int d\tilde{x} \left\{ -[\tilde{q}(\tilde{x}) + \tilde{n}_0(\tilde{x})]^2 - \frac{1}{2} \tilde{n}_0^2(\tilde{x}) - \sqrt{\tilde{n}_0(\tilde{x})} \right. \\ \left\{ \tilde{\mu} + \left(\frac{\xi}{R_{\text{TF}}} \right)^2 \frac{\partial^2}{\partial \tilde{x}^2} - 2[\tilde{q}(\tilde{x}) + \tilde{n}_0(\tilde{x})] - \tilde{x}^2 \right. \\ \left. + 2\tilde{D}\tilde{Q}_0(\tilde{x}) \right\} \sqrt{\tilde{n}_0(\tilde{x})} + 2\tilde{D}\tilde{Q}_0(\tilde{x}) [\tilde{q}(\tilde{x}) + \tilde{n}_0(\tilde{x})] \\ - 2\tilde{D} \frac{\tilde{q}(\tilde{x}) + \tilde{n}_0(\tilde{x})}{\sqrt{-\tilde{\mu} + 2[\tilde{q}(\tilde{x}) + \tilde{n}_0(\tilde{x})] + \tilde{x}^2 - 2\tilde{D}\tilde{Q}_0(\tilde{x})}} \right\}, \quad (36)$$

where $\tilde{\mathcal{F}} = \mathcal{F}/(\bar{\mu}nR_{\text{TF}})$ denotes the dimensionless free energy and $\tilde{Q}_0(\tilde{x}) = \sqrt{\frac{2\tilde{\mu}}{M}} Q_0(x)$.

Motivated by the analytical and the numerical results presented in Figs. 2 and 5, respectively, we suggest the three following ansätze for the condensate density $\tilde{n}_0(\tilde{x})$, the Bose-glass order parameter $\tilde{q}(\tilde{x})$, and the auxiliary function $\tilde{Q}_0(\tilde{x})$:

$$\tilde{n}_0(\tilde{x}) = \alpha e^{-\sigma \tilde{x}^2}, \quad (37)$$

$$\tilde{q}(\tilde{x}) + \tilde{n}_0(\tilde{x}) = \gamma e^{-\theta \tilde{x}^2}, \quad (38)$$

$$\tilde{Q}_0(\tilde{x}) = \frac{\tilde{q}(\tilde{x}) + \tilde{n}_0(\tilde{x})}{\tilde{D}} - (\zeta + \eta \tilde{x}^2), \quad (39)$$

where α , σ , γ , θ , ζ , and η denote variational parameters. The parameters α and γ are proportional to the number of particles in the condensate and the total number of particles, while parameters σ and θ represent the width of the condensate density and the total density, respectively.

Inserting the ansätze (37)–(39) into the free energy (36) and performing the integral yield:

$$\tilde{\mathcal{F}} = \sqrt{\pi} \left\{ \frac{\gamma^2}{\sqrt{2\theta}} + \frac{\alpha}{2\sigma^{3/2}} - \frac{\alpha}{4\sqrt{\sigma}} (4\tilde{\mu} + \sqrt{2}\alpha) \right. \\ \left. + \left(\frac{\xi}{R_{\text{TF}}} \right)^2 \frac{\alpha\sqrt{\sigma}}{2} + \tilde{D} \left(\frac{2\alpha\zeta}{\sqrt{\sigma}} + \frac{\alpha\eta}{\sigma^{3/2}} - \frac{\gamma(\eta + 2\zeta\theta)}{\theta^{3/2}} \right) \right. \\ \left. - \frac{2\tilde{D}\gamma}{\sqrt{1 + 2\tilde{D}\eta}} e^{\frac{2\tilde{D}\zeta - \tilde{\mu}}{2 + 4\tilde{D}\eta}\theta} K_0 \left(\frac{2\tilde{D}\zeta - \tilde{\mu}}{2 + 4\tilde{D}\eta} \theta \right) \right\}, \quad (40)$$

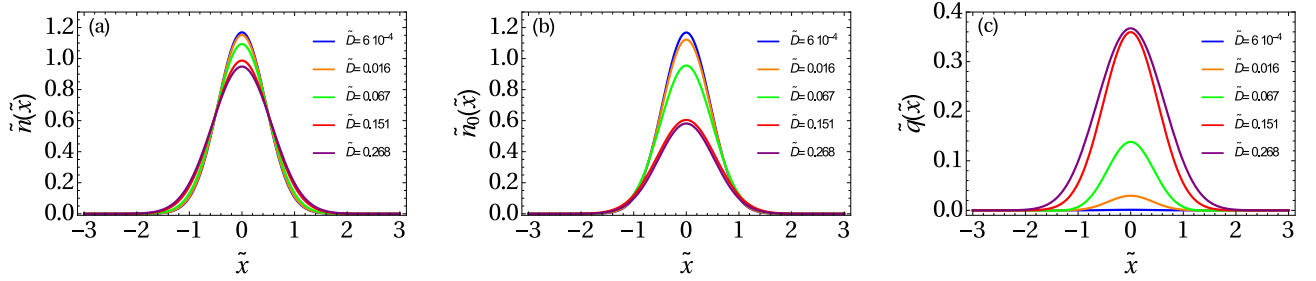


Figure 8: (Color online) Spatial distribution of: (a) particle density $\tilde{n}(\tilde{x})$, (b) condensate density $\tilde{n}_0(\tilde{x})$, and (c) Bose-glass order parameter $\tilde{q}(\tilde{x})$ for increasing disorder strengths \tilde{D} , from the top to the bottom in the center in (a) and (b), and from the bottom to the top in (c).

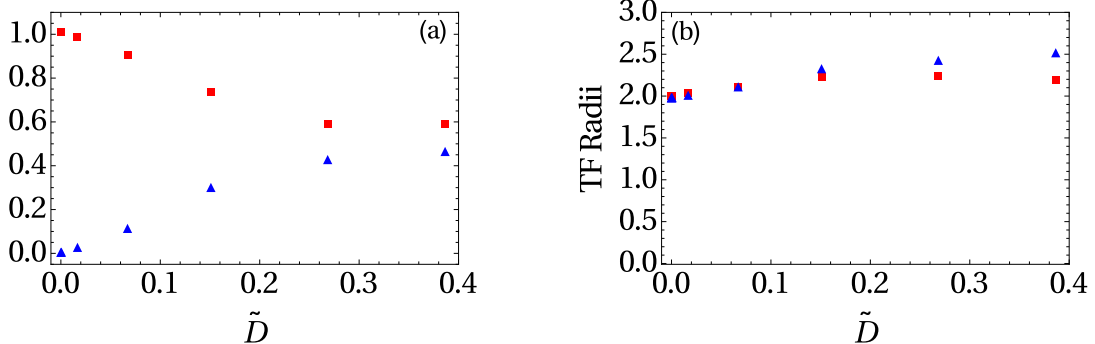


Figure 9: (Color online) (a) Fractional number of condensed particles N_0/N (square, red) and fractional number of particles Q/N in the disconnected local mini-condensates (triangle, blue) and (b) condensate radius \tilde{R}_{TF1} (square, red) and cloud radius \tilde{R}_{TF2} (triangle, blue), as a function of disorder strength \tilde{D} .

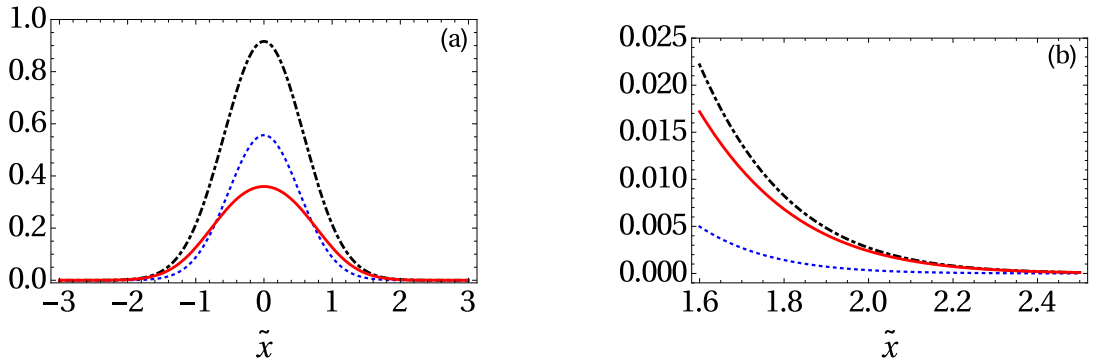


Figure 10: (Color online) Spatial distribution of: (a) particle density $\tilde{n}(\tilde{x})$ (dotted-dashed, black), condensate density $\tilde{n}_0(\tilde{x})$ (dotted, blue), Bose-glass order parameter $\tilde{q}(\tilde{x})$ (solid, red) and (b) blow-up of the border region for $\tilde{D} = 0.386$.

where $K_0(s)$ represents the modified Bessel function of the second kind.

The free energy (40) has now to be extremized with respect to the variational parameters α , σ , γ , θ , ζ , and η . Together with the thermodynamic condition $-\frac{\partial \tilde{F}}{\partial \tilde{\mu}} = \frac{4}{3}$, we have seven coupled equations for seven variables α , σ , γ , θ , ζ , η , and $\tilde{\mu}$ that we solve numerically. From all physical solutions we select the one with the smallest free energy (40), then we insert the resulting variational parameters α , σ , γ , and θ into the ansätze (37) and (38) in

order to get the total density $\tilde{n}(\tilde{x})$, the condensate density $\tilde{n}_0(\tilde{x})$, and the Bose-glass order parameter $\tilde{q}(\tilde{x})$. In Fig. 8(a) we see that the density of bosons has a Gaussian shape and vanishes at the cloud radius \tilde{R}_{TF2} . The maximal value of the total density decreases with the disorder strength, while its width increases. The condensate density $\tilde{n}_0(\tilde{x})$ in Fig. 8(b) has the same qualitative behavior as the total density $\tilde{n}(\tilde{x})$ in Fig. 8(a) and vanishes at the condensate radius \tilde{R}_{TF1} . The response of the condensate density $\tilde{n}_0(\tilde{x})$ to disorder can be clearly seen in Fig. 9(a),

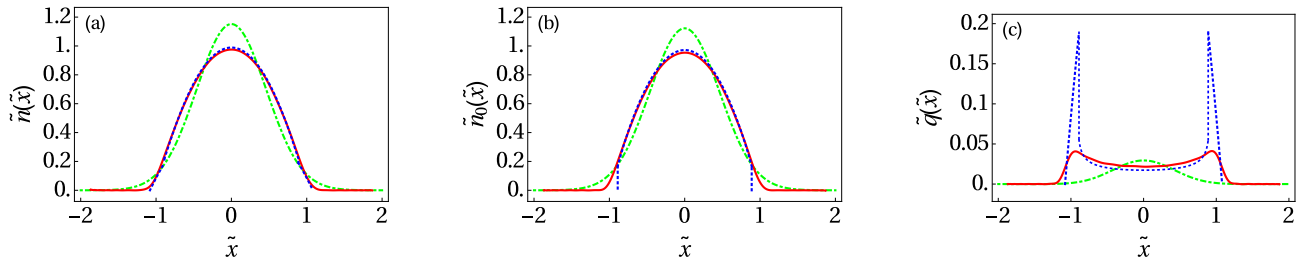


Figure 11: (Color online) Spatial distribution of (a) total particle density $\tilde{n}(\tilde{x})$, (b) condensate density $\tilde{n}_0(\tilde{x})$, and (c) Bose-glass order parameter $\tilde{q}(\tilde{x})$: variational (dotted-dashed, green), numerical (solid, red), and analytical (dotted, blue) for $\tilde{D} = 0.016$.

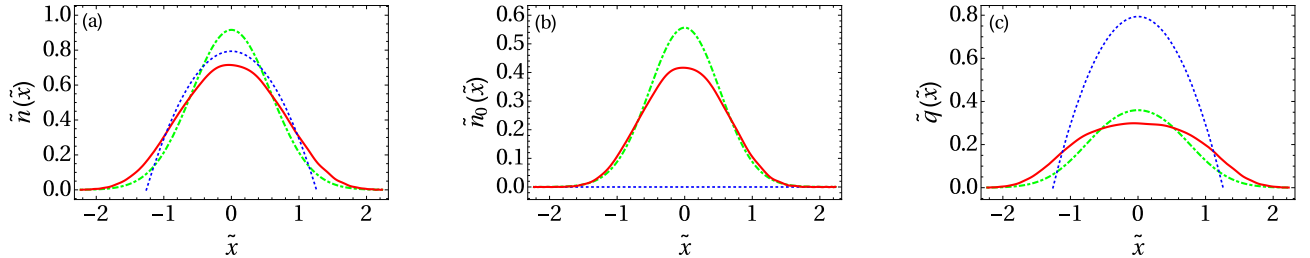


Figure 12: (Color online) Spatial distribution of (a) total particle density $\tilde{n}(\tilde{x})$, (b) condensate density $\tilde{n}_0(\tilde{x})$, and (c) Bose-glass order parameter $\tilde{q}(\tilde{x})$: variational (dotted-dashed, green), numerical (solid, red), and analytical (dotted, blue) results for $\tilde{D} = 0.386$.

where the fractional number of condensed particles N_0/N is plotted as a function of the disorder strength. In the clean case all particles are in the condensate, but as we increase the disorder strength, more and more particles leave the condensate. Starting from the disorder strength value $\tilde{D} = 0.393$, the variational equations turn out to have only complex solutions, so we do not have any information about our system for higher disorder strengths. Thus, we can not predict if, at a certain critical disorder strength, the condensate density would vanish.

The Bose-glass order parameter $\tilde{q}(\tilde{x})$ in Fig. 8(c) has a similar shape as $\tilde{n}(\tilde{x})$ and $\tilde{n}_0(\tilde{x})$. When we increase the disorder strength, the maximal value of the Bose-glass order parameter density as well as its width increases. Better understanding of the influence of the disorder on the local mini-condensates can be deduced from Fig. 9(a), where the fractional number of particles Q/N in the disconnected local mini-condensates is zero in the clean case, and then increases with \tilde{D} . This means that more bosons are going into the local minima of the disorder potential when we increase the disorder strength. Due to the fact that physical solutions exist only in a limited range of the disorder strength, we are not able to predict if there exists a critical disorder strength value, where all particles leave the condensate and fill the local mini-condensates only. In order to determine whether the bosonic cloud contains beside the superfluid region also a Bose-glass region, we plot the total density $\tilde{n}(\tilde{x})$, the condensate density $\tilde{n}_0(\tilde{x})$, and the Bose-glass order parameter $\tilde{q}(\tilde{x})$ together in Fig. 10(a) for the disorder strength value $\tilde{D} = 0.386$. The blow-up of the border region in

Fig. 10(b) shows clearly that the condensate density vanishes, while the Bose-glass order parameter still persists, which is the definition of the Bose-glass region. The cloud radius $\tilde{R}_{\text{TF}2}$ and the condensate radius $\tilde{R}_{\text{TF}1}$ are defined by the length where the total density and the condensate density are equal to 10^{-4} , respectively. Both radii are identical in the weak-disorder regime in Fig. 9(b), and both are increasing with the disorder strength. But we can not determine if, for higher disorder strengths, they will keep increasing, remain constant, or the condensate radius $\tilde{R}_{\text{TF}1}$ vanishes, i.e., we can not say if a quantum phase transition exists or not.

V. COMPARISON OF ANALYTICAL, NUMERICAL AND VARIATIONAL RESULTS

Now we compare the physical quantities obtained via the three different methods: the TF approximation, the numerical method, and the variational method. For the small disorder strength $\tilde{D} = 0.016$, the three total densities $\tilde{n}(\tilde{x})$ in Fig. 11(a) agree qualitatively well, but quantitatively the TF-approximated $\tilde{n}(\tilde{x})$ is still the best approximation for the numerical total density, especially in the center of the bosonic cloud, where the variational result does not agree well with the numerical one. The same remark can be made for the condensate density $\tilde{n}_0(\tilde{x})$ in Fig. 11(b). For the Bose-glass order parameter $\tilde{q}(\tilde{x})$ in Fig. 11(c) the double-bump structure, which exists in both numerical and TF approximated results, is missing in the variational result, which has just a bell

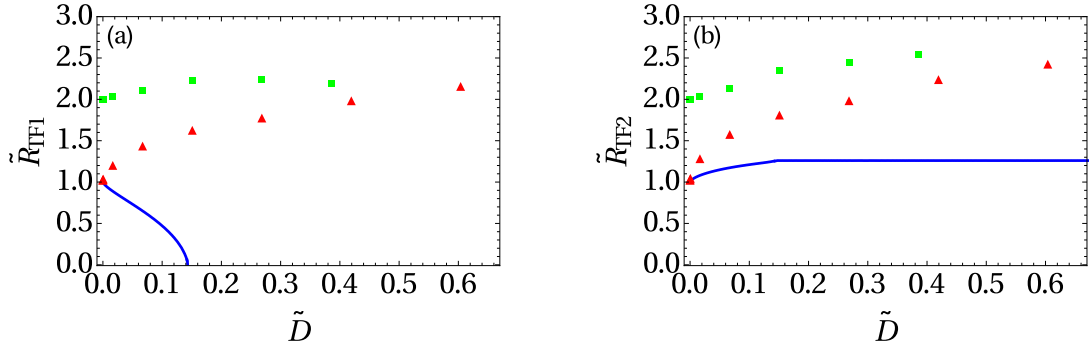


Figure 13: (Color online) Analytical (solid, blue), numerical (triangle, red), and variational (square, green) results for (a) condensate radius $\tilde{R}_{\text{TF}1}$ and (b) cloud radius $\tilde{R}_{\text{TF}2}$, as functions of the disorder strength \tilde{D} .

form by definition. This makes again the TF-approximated Bose-glass order parameter $\tilde{q}(\tilde{x})$ the best approximation for the numerical one. For the intermediate disorder strength $\tilde{D} = 0.386$, the TF-approximated total density $\tilde{n}(\tilde{x})$ in Fig. 12(a) is also the best approximation for the numerical one in the center of the bosonic cloud, while at the border of the trap the variational and the numerical total density agree well. According to the TF approximation shown in Fig. 3, we are at the disorder strength value $\tilde{D} = 0.386$ already in the Bose-glass phase, thus, the TF-approximated condensate density $\tilde{n}_0(\tilde{x})$ in Fig. 12(b) vanishes. This is not the case for both the numerical and the variational condensate densities, which are compatible and match at the borders of the trap. The variational Bose-glass order parameter $\tilde{q}(\tilde{x})$ also agrees well with the numerical one and both have the same bell shape, while the TF approximated Bose-glass order parameter has a significant deviation, which is expected since the TF-approximation breaks down in the intermediate disorder regime. In Fig. 13(a) the variational and the numerical condensate radius $\tilde{R}_{\text{TF}1}$ have the same behavior, both increase with the disorder strength, contrarily to the analytical result for the condensate radius, which decreases with \tilde{D} . Furthermore, the analytical results for $\tilde{R}_{\text{TF}1}$ indicate the existence of a quantum phase transition, while the variational and the numerical treatments break down at a certain critical value of the disorder strength before it could be deduced whether the quantum phase transition exists at larger disorder strength. In the weak disorder regime, the analytical and the numerical condensate radii are comparable, while in the intermediate disorder regime the variational and the numerical condensate radii are the ones which agree qualitatively.

Figure 13(b) shows that in the weak disorder regime, the variational, the numerical, and the analytical cloud radii agree qualitatively, since the three of them increase with the disorder strength, with a convergence of the variational and the numerical radii for larger \tilde{D} . In the intermediate disorder regime the analytical cloud radius remains constant, but both the variational and the nu-

merical cloud radii keep increasing for accessible disorder strength. Since current approaches break down for sufficient large \tilde{D} , other approaches are needed for tackling the regime of strong disorder.

VI. CONCLUSIONS

From the discussion in the previous section, we conclude that the TF approximation yields good results for the quasi one-dimensional dirty bosons in the weak disorder regime, which agree well with the numerical ones, especially in the center of the bosonic cloud, where the kinetic energy can be neglected. However, this approximation breaks down in the intermediate disorder regime, and is unable to describe the BEC system properly. On the other side, the variational method with the ansätze (37)–(39) turns out to be a good approximation to describe the BEC system in the intermediate disorder regime and works there better than in the weak one, especially at the border of the cloud, where the Bose-glass region is located. This is due to the fact that a stronger disorder reduces significantly the repulsive interaction between the particles and approaches the case of non-interacting bosons, where the densities are Gaussian, as in our variational ansätze. Although the variational method does not provide physical results for larger disorder strengths, it still treats an important range of the disorder strength. The combination of applying the TF approximation for the weak disorder regime together with the variational method for the intermediate disorder regime covers a significant range of disorder strengths. With this we explain analytically the redistribution of the minicondensates from the edge of the atomic cloud to the trap center for increasing disorder strengths as obtained from detailed numerical simulations. We expect that all these results are useful for a quantitative analysis of experiments for dirty bosons in quasi one-dimensional harmonic traps. The problem of the large disorder strengths still persists with the current approach and remains to be addressed by other methods.

Acknowledgments

The authors gratefully acknowledge financial support from German Academic and Exchange Service (DAAD), the Ministry of Education, Science, and Technological Development of the Republic of Serbia under projects ON171017, NAI-DBEC, and IBEC, and German Research Foundation (DFG) via the Collaborative Research

Center SFB/TR49 “Condensed Matter Systems with Variable Many-Body Interactions”.

Numerical simulations were run on the PARADOX supercomputing facility at the Scientific Computing Laboratory of the Institute of Physics Belgrade, supported in part by the Ministry of Education, Science, and Technological Development of the Republic of Serbia under project ON171017.

[1] M. P. A. Fisher, P. B. Weichman, G. Grinstein, and D. S. Fisher, Phys. Rev. B **40**, 546 (1989).

[2] B. C. Crooker, B. Hebral, E. N. Smith, Y. Takano, and J. D. Reppy, Phys. Rev. Lett. **51**, 666 (1983).

[3] R. Folman, P. Krüger, J. Schmiedmayer, J. Denschlag, and C. Henkel, Adv. At. Mol. Opt. Phys. **48**, 263 (2002).

[4] D. W. Wang, M. D. Lukin, and E. Demler, Phys. Rev. Lett. **92**, 076802 (2004).

[5] T. Schumm, J. Esteve, C. Figl, J. B. Trebbia, C. Aussibal, H. Nguyen, D. Mailly, I. Bouchoule, C. I. Westbrook, and A. Aspect, Eur. Phys. J. D **32**, 171 (2005).

[6] J. Fortágh and C. Zimmermann, Rev. Mod. Phys. **79**, 235 (2007).

[7] P. Krüger, L. M. Andersson, S. Wildermuth, S. Hofferberth, E. Haller, S. Aigner, S. Groth, I. Bar-Joseph, and J. Schmiedmayer, Phys. Rev. A **76**, 063621 (2007).

[8] J. E. Lye, L. Fallani, M. Modugno, D. S. Wiersma, C. Fort, and M. Inguscio, Phys. Rev. Lett. **95**, 070401 (2005).

[9] D. Clément, A. F. Varón, M. Hugbart, J. A. Retter, P. Bouyer, L. Sanchez-Palencia, D. M. Gangardt, G. V. Shlyapnikov, and A. Aspect, Phys. Rev. Lett. **95**, 170409 (2005).

[10] J. C. Dainty (Ed.), *Laser Speckle and Related Phenomena*, Springer, Berlin, 1975.

[11] J. W. Goodman, *Speckle Phenomena in Optics: Theory and Applications*, Viva Books Private Limited, First Edition, 2010.

[12] J. Billy, V. Josse, Z. Zuo, A. Bernard, B. Hambrecht, P. Lugan, D. Clement, L. Sanchez-Palencia, P. Bouyer, and A. Aspect, Nature (London) **453**, 891 (2008).

[13] U. Gavish and Y. Castin, Phys. Rev. Lett. **95**, 020401 (2005).

[14] B. Gadway, D. Pertot, J. Reeves, M. Vogt, and D. Schneble, Phys. Rev. Lett. **107**, 145306 (2011).

[15] B. Damski, J. Zakrzewski, L. Santos, P. Zoller, and M. Lewenstein, Phys. Rev. Lett. **91**, 080403 (2003).

[16] T. Schulte, S. Drenkelforth, J. Kruse, W. Ertmer, J. Arlt, K. Sacha, J. Zakrzewski, and M. Lewenstein, Phys. Rev. Lett. **95**, 170411 (2005).

[17] G. Roati, C. D’Errico, L. Fallani, M. Fattori, C. Fort, M. Zaccanti, G. Modugno, M. Modugno, and M. Inguscio, Nature (London) **453**, 895 (2008).

[18] P. W. Anderson, Phys. Rev. **109**, 1492 (1958).

[19] K. Huang and H. F. Meng, Phys. Rev. Lett. **69**, 644 (1992).

[20] S. Giorgini, L. Pitaevskii, and S. Stringari, Phys. Rev. B **49**, 12938 (1994).

[21] M. Kobayashi and M. Tsubota, Phys. Rev. B **66**, 174516 (2002).

[22] A. V. Lopatin and V. M. Vinokur, Phys. Rev. Lett. **88**, 235503 (2002).

[23] G. M. Falco, A. Pelster, and R. Graham, Phys. Rev. A **75**, 063619 (2007).

[24] C. Krumnow and A. Pelster, Phys. Rev. A **84**, 021608(R) (2011).

[25] B. Abdullaev and A. Pelster, Europ. Phys. J. D **66**, 314 (2012).

[26] B. Nikolic, A. Balaz, and A. Pelster, Phys. Rev. A **88**, 013624 (2013).

[27] M. Ghabour and A. Pelster, Phys. Rev. A **90**, 063636 (2014).

[28] A. Boudjemaa, Phys. Rev. A **91**, 053619 (2015).

[29] C. Gaul and C. A. Muller, Phys. Rev. A **83**, 063629 (2011).

[30] C. A. Muller and C. Gaul, New J. Phys. **14**, 075025 (2012).

[31] P. Navez, A. Pelster, and R. Graham, App. Phys. B **86**, 395 (2007).

[32] V. I. Yukalov and R. Graham, Phys. Rev. A **75**, 023619 (2007).

[33] V. I. Yukalov, E. P. Yukalova, K. V. Krutitsky, and R. Graham, Phys. Rev. A **76**, 053623 (2007).

[34] T. Nattermann and V. L. Pokrovsky, Phys. Rev. Lett. **100**, 060402 (2008).

[35] G. M. Falco, T. Nattermann, and V. L. Pokrovsky, Phys. Rev. B **80**, 104515 (2009).

[36] R. Graham and A. Pelster, Int. J. Bif. Chaos **19**, 2745 (2009).

[37] V. Dotsenko, *An Introduction to the Theory of Spin Glasses and Neural Networks*, World Scientific, Singapore, 1994.

[38] G. Parisi, J. Phys. France **51**, 1595 (1990).

[39] M. Mezard and G. Parisi, J. Phys. I France **1**, 809 (1991).

[40] T. Khellil and A. Pelster, in preparation.

[41] H. Perrin, Y. Colombe, B. Mercier, V. Lorent, and C. Henkel, J. Phys. B: At. Mol. Opt. Phys. **39**, 4649 (2006).

[42] R. Carretero-González, D. J. Frantzeskakis, and P. G. Kevrekidis, Nonlinearity **21**, R139 (2008).

[43] M. Mezard, G. Parisi, and M. A. Virasoro, World Scientific, Singapore, 1986.

[44] A. J. Leggett, *Quantum Liquids: Bose Condensation and Cooper Pairing in Condensed-Matter Systems*, Oxford Graduate Texts, Oxford, 2006.

[45] S. Sachdev, *Quantum Phase Transitions*, Second Edition, Cambridge University Press, Cambridge, 2011.

[46] K. H. Fischer and J. A. Hertz, *Spin Glasses*, Cambridge University Press, Cambridge, 1991.

[47] S. F. Edwards and P. W. Anderson, J. Phys. F: Met. Phys. **5**, 965 (1975).

[48] A. I. Larkin, Zh. Eksp. Theor. Fiz. **58**, 1466 (1970).

[49] J. Majda and P. Kramer, Phys. Rep. **314**, 237 (1999).

- [50] M. Düttmann, Diploma Thesis, Freie Universität Berlin, Germany (2009). <http://users.physik.fu-berlin.de/~pelster/Theses/duettmann.pdf>
- [51] W. H. Press, S. A. Teukolsky, W. T. Vetterling, B. P. Flannery, *Numerical Recipes: The Art of Scientific Computing*, Third Edition, Cambridge University Press, Cambridge, 2007.
- [52] P. Muruganandam and S.K. Adhikari, *Comput. Phys. Commun.* **180**, 1888 (2009).
- [53] D. Vudragović, I. Vidanović, A. Balaž, P. Muruganandam, and S. Adhikari, *Comput. Phys. Commun.* **183**, 2021 (2012).
- [54] R. Kishor Kumar, L. E. Young-S, D. Vudragović, A. Balaž, P. Muruganandam, and S.K. Adhikari, *Comput. Phys. Commun.* **195**, 117 (2015).
- [55] V. M. Pérez-Garcia, H. Michinel, J. I. Cirac, M. Lewenstein, and P. Zoller, *Phys. Rev. Lett.* **77**, 5320 (1996).
- [56] V. M. Pérez-Garcia, H. Michinel, J. I. Cirac, M. Lewenstein, P. Zoller, *Phys. Rev. A*, **56**, 1424 (1997).
- [57] H. Kleinert and V. Schulte-Frohlinde, *Critical Properties of Φ^4 -Theories*, World Scientific, Singapore, 2001.
- [58] H. Kleinert, *Path Integrals in Quantum Mechanics, Statistics, Polymer Physics, and Financial Markets*, Fifth Edition, World Scientific, Singapore, 2009.